Journal of Power Sources 230 (2013) 89–95

Contents lists available at SciVerse ScienceDirect

Journal of Power Sources

journal homepage: www.elsevier.com/locate/jpowsour

Preparation and characterization of size-uniform $Li[Li_{0.131}Ni_{0.304}Mn_{0.565}]O_2$ particles as cathode materials for high energy lithium ion battery

Xingde Xiang [a], Xiaoqing Li [b], Weishan Li [a,b,*]

[a] School of Materials Science and Engineering, South China University of Technology, Guangzhou 510640, China
[b] School of Chemistry and Environment, South China Normal University, Guangzhou 510006, China

HIGHLIGHTS

- $Li[Li_{0.131}Ni_{0.304}Mn_{0.565}]O_2$ was prepared by PVP and EG-assisted co-precipitation.
- Prepared sample delivers a high capacity with good cycle stability and rate performance.
- Capacity decay is related to solubility and structural rearrangement of metal ions.

ARTICLE INFO

Article history:
Received 24 October 2012
Received in revised form
6 December 2012
Accepted 11 December 2012
Available online 20 December 2012

Keywords:
Lithium ion battery
Lithium-rich layered oxide
Preparation
Particle size
Capacity decay

ABSTRACT

Lithium-rich layered oxide, $Li[Li_{0.131}Ni_{0.304}Mn_{0.565}]O_2$ with uniform particle size, is prepared through co-precipitation of metal hydroxide with synergistic dispersion of polyvinylpyrrolidone and ethylene glycol and subsequent solid reaction with lithium hydroxide. The crystal structure and morphology of the prepared sample is characterized with X-ray diffraction and scanning electron microscope. It is found that the prepared sample is a solid solution of Li_2MnO_3 and $LiNi_{0.5}Mn_{0.5}O_2$, with uniform particle size of about 230 nm. Charge/discharge tests indicate that the prepared sample exhibits improved elevated-temperature discharge capacity and cycling stability. In the region of 3.0–4.8 V, the prepared sample delivers initially a 0.1 C (1 C = 263 mAh g^{-1}) capacity of 256 mAh g^{-1} at 50 °C and 205 mAh g^{-1} at 25 °C, and the 0.1 C capacity at 25 °C retains 178 mAh g^{-1} after 60 cycles. The capacity decay mechanism is understood in detail through d*Q*/d*V* analyses.

1. Introduction

Electrochemical devices are needed for the energy storage in electronic products, electric vehicles and renewable energy exploitation [1]. Among all the electrochemical devices for energy storage, lithium ion battery is considered to be the most promising technology, because it has high energy density and long lifetime [2]. However, the energy density of lithium ion battery based on current technology is not high enough for its commercial application, especially in electric vehicles. To improve the energy density of lithium ion battery, new materials are necessary. For example, anode materials with low potential and high specific capacity and cathode materials with high potential and high specific capacity need to be developed. Unlike the anode materials that have many candidates, few cathode materials are available for high energy lithium ion battery.

Cathode materials used in current lithium ion battery deliver low specific capacity, such as $LiCoO_2$ (~145 mAh g^{-1}) [3], $LiMn_2O_4$ (~120 mAh g^{-1}) [4,5], $LiFePO_4$ (~140 mAh g^{-1}) [6] and $LiNi_{1/3}Co_{1/3}Mn_{1/3}O_2$ (~160 mAh g^{-1}) [7]. Lithium-rich layered oxide ($Li[Li_{1/3-2x/3}Ni_xMn_{2/3-x/3}]O_2$, $0 < x < 0.5$) is believed to be a promising cathode material for high energy lithium ion battery, because they could deliver a specific capacity over 200 mAh g^{-1} with an operating potential higher than 3.5 V (*vs* Li/Li^+) in average [8]. Much work has been done for the preparation and characterization of lithium-rich layered oxides [8–24]. Jarvis et al. proved that $Li[Li_{1/3-2x/3}Ni_xMn_{2/3-x/3}]O_2$ was composed of a solid solution with a C2/m monoclinic symmetry and multiple planar defects by combining aberration-corrected scanning transmission electron microscopy (STEM), computation simulations and diffraction scanning transmission electron microscopy (D-STEM) [12]. Armstrong et al. employed in situ differential electrochemical mass spectrometry (DEMS) and powder neutron diffraction to

* Corresponding author. School of Chemistry and Environment, South China Normal University, Guangzhou 510006, China. Tel./fax: +86 20 39310256.
E-mail address: liwsh@scnu.edu.cn (W. Li).

0378-7753/$ – see front matter © 2012 Elsevier B.V. All rights reserved.
http://dx.doi.org/10.1016/j.jpowsour.2012.12.050

demonstrate that oxygen would evolve from the surface of lithium-rich oxides when the charge potential was above 4.5 V in the first cycle, and the oxygen loss was accompanied by diffusion of transition metal ions from surface to bulk where they occupy vacancies created by Li removal [14]. Electrochemical behavior and thermal stability of $Li[Li_{1/3-2x/3}Ni_xMn_{2/3-x/3}]O_2$ with different x values were investigated in detail by Dahn's group [8,9,17]. $Li[Li_{1/3-2x/3}Ni_xMn_{2/3-x/3}]O_2$ with low capacity loss was developed through coating and doping by Manthiram's group [20,21]. However, $Li[Li_{1/3-2x/3}Ni_xMn_{2/3-x/3}]O_2$ materials used in these studies were prepared by traditional co-precipitation, in which metal hydroxide precursor was formed by dropping alkaline solution into metal ion containing solution without using any dispersant, resulting in non-uniform particle sizes that do not favor understanding the capacity decay mechanism of $Li[Li_{1/3-2x/3}Ni_xMn_{2/3-x/3}]O_2$ with cycling.

In this work, we proposed a new method for preparing lithium-rich layered oxide with uniform particle size, in which polyvinylpyrrolidone (PVP) and ethylene glycol (EG) were introduced as dispersants. A representational lithium-rich layered oxide, $Li[Li_{0.131}Ni_{0.304}Mn_{0.565}]O_2$, was prepared and characterized with X-ray diffraction, scanning electron microscope and charge–discharge test.

2. Experimental

2.1. Preparation

Precursor-controlled synthesis is usually effective for preparing lithium-intercalated cathode material with high performance, although the precursor will be subsequently treated at high temperature [25,26]. To obtain lithium-rich layered oxide with uniform particles size, we propose to control the growth of the transition metal hydroxide precursor with synergistic dispersion of PVP and EG. As a non-ionic surfactant, PVP forms micella in aqueous solution and limits the growth space of particles. Ethylene glycol has high viscosity and restricts the growth rate of particles. The formation process of the lithium-rich layered oxide is shown in Scheme 1.

Typically, 1 g PVP was dispersed under magnetic stirring in the mixed solvent of 60 ml distilled water and 20 ml ethylene glycol. Subsequently, 10 g manganese acetate ($Mn(CH_3COO)_2\cdot 4H_2O$) and 5.46 g nickel acetate $Ni(CH_3COO)_2\cdot 4H_2O$ were added. After continuous stirring for 1 h, 57 ml 2.67 mol L^{-1} lithium hydroxide aqueous solution was added slowly for the formation of transition metal hydroxide ($Ni_{0.35}Mn_{0.65}(OH)_2$) precipitation, and the reaction time was 12 h. The precipitation was centrifuged, washed, filtrated, and dried in vacuum at 100 °C. All chemicals were obtained from Aladin agents corporation (Wuhan, China).

As a precursor, $Ni_{0.35}Mn_{0.65}(OH)_2$ was mixed uniformly with lithium hydroxide in a required amount, and then transferred into a muffle furnace. The mixture was calcined at 450 °C for 4 h and then at 900 °C for 8 h and finally the product $Li[Li_{0.131}Ni_{0.304}Mn_{0.565}]O_2$ was obtained. The heating rate from room temperature to 450 °C and from 450 °C to 900 °C was 3 °C min^{-1}. Moreover, $LiNi_{0.5}Mn_{0.5}O_2$ and Li_2MnO_3 were also carefully prepared for XRD comparison as similar steps.

2.2. Characterization

The morphology of $Ni_{0.35}Mn_{0.65}(OH)_2$, and $Li[Li_{0.131}Ni_{0.304}Mn_{0.565}]O_2$ was observed by scanning electron microscope (JSM-6380, Japan), and scanning electron microscope (ZEISS Ultra 55, Germany), respectively. The crystal structures of the samples were analyzed by X-ray diffraction (BRUKER D8 ADVANCE, Germany) with Cu K_α radiation.

2.3. Electrochemical measurements

The electrode was prepared by mixing 80 wt% active material ($Li[Li_{0.131}Ni_{0.304}Mn_{0.565}]O_2$) with 10 wt% acetylene black and 10 wt% poly(tetrafluoroethylene) binder, coating the mixture on an aluminum sheet, and then cutting the sheet into pieces with 1 cm × 1 cm. The CR2032 coin cell was assembled in an Ar-filled glove box (Mikrouna, Super 1220/750/900) by using prepared electrode as cathode, lithium film as anode, Celgard 2400 as separator and 1 M $LiPF_6$ in EC:DMC (1:1 in volume) as electrolyte. The charge/discharge test was performed on Land cell test system (Land CT 2001A, China).

3. Results and discussion

3.1. Crystal structure and morphology

The morphology of the resultant precursor $Ni_{0.35}Mn_{0.65}(OH)_2$ was observed by SEM and Fig. 1 presents the observed result. As seen from Fig. 1, the precursor is composed of particles with an average size of about 100 nm, showing the contribution of PVP and EG for the formation of uniform $Ni_{0.35}Mn_{0.65}(OH)_2$ particles. It has been known that the crystal structure of nickel and manganese hydroxide is related to its composition [27]. To identify the composition of the precursor, X-ray diffraction was performed. Fig. 2 presents the XRD

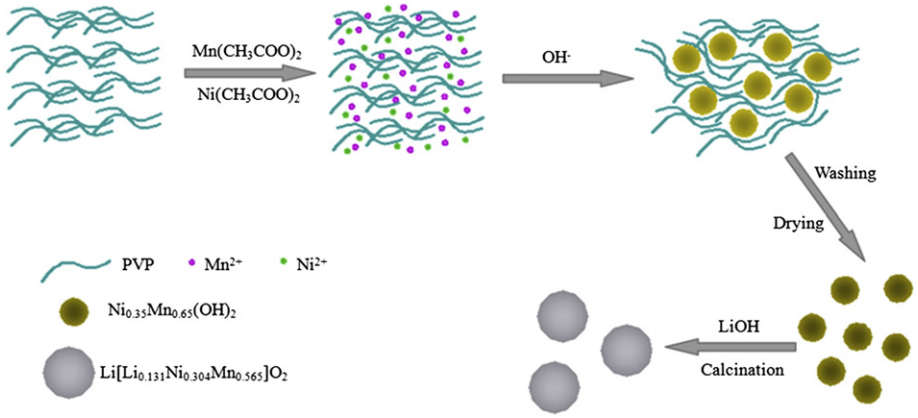

Scheme 1. Schematic formation process of $Li[Li_{0.131}Ni_{0.304}Mn_{0.565}]O_2$ particles.

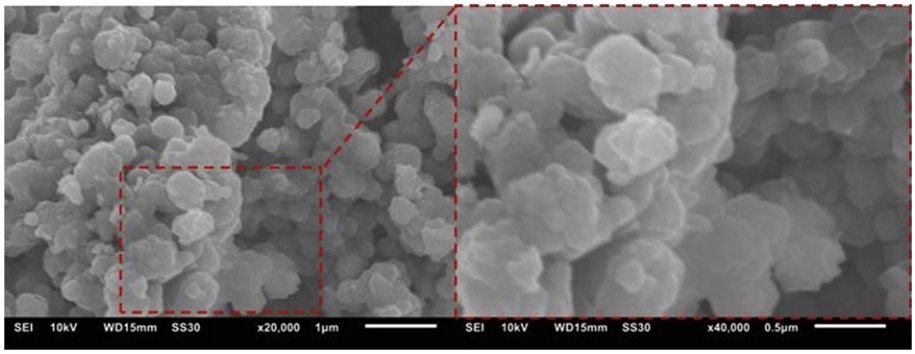

Fig. 1. SEM images of $Ni_{0.35}Mn_{0.65}(OH)_2$.

pattern of the precursor, which can be matched well with *P-3m1* space group (PDF#14-0117), *P* space group (PDF#18-0803) and *I41/amd* space group (PDF#18-0804). The main peaks matched with *P-3m1* space group correspond to metal hydroxide with CdI_2-type structure [27], while other sharp peaks matched with *P* space group and *I41/amd* space group can be assigned to hydroxide metal oxide ($Ni_xMn_{1-x}OOH$) with Feitknechtite structure and $(Ni_xMn_{1-x})_3O_4$ with Hausmannite structure, respectively.

Fig. 3 presents the XRD pattern of the prepared $Li[Li_{0.131}Ni_{0.304}Mn_{0.565}]O_2$ compared with those of $LiNi_{0.5}Mn_{0.5}O_2$ and Li_2MnO_3. $Li[Li_{0.131}Ni_{0.304}Mn_{0.565}]O_2$ shows nine sharp peaks located at 18.7°, 36.7°, 38.4°, 44.4°, 48.6°, 58.6°, 64.3°, 65.0°, and 68.3°, respectively, and some other weak peaks at 21°–25° and at 75°–80°, very similar to the pattern of lithium-rich layered oxides reported in literature [8,9]. The weak peaks at 20°–30° are the characteristic of Li_2MnO_3-type structure with $LiMn_6$ (or Ni-substituted) cation arrangements in the transition metal layers [11,24]. Although many observations have been made for $Li[Li_{1/3-2x/3}Ni_xMn_{2/3-x/3}]O_2$, its microstructure is still not clear. Some researchers argue that it is a solid solution built with C/2m symmetry, according to the STEM observation and ED analysis [12,28]. Others believed that it was an integrated composite of $LiNi_{0.5}Mn_{0.5}O_2$ with $R\bar{3}m$ symmetry and Li_2MnO_3 with C/2m symmetry, which was also supported by STEM results [29,30]. Comparing the XRD patterns of $Li[Li_{0.131}Ni_{0.304}Mn_{0.565}]O_2$, $LiNi_{0.5}Mn_{0.5}O_2$ and Li_2MnO_3 in Fig. 3, it can be known that there is a little difference in the peak positions of these three samples. The peak positions of $Li[Li_{0.131}Ni_{0.304}Mn_{0.565}]O_2$ are just located between those of $LiNi_{0.5}Mn_{0.5}O_2$ and Li_2MnO_3, as shown in Table 1. Therefore, we can infer that the prepared $Li[Li_{0.131}Ni_{0.304}Mn_{0.565}]O_2$ is a solid solution of $LiNi_{0.5}Mn_{0.5}O_2$ and Li_2MnO_3.

The morphology of the prepared $Li[Li_{0.131}Ni_{0.304}Mn_{0.565}]O_2$ was observed by scanning electron microscope. The SEM images and particle size distribution are shown in Fig. 4. It can be seen from Fig. 4 that the particles of the prepared $Li[Li_{0.131}Ni_{0.304}Mn_{0.565}]O_2$ are polygonal and very uniform with an average size of 230 nm. This confirms that $Li[Li_{0.131}Ni_{0.304}Mn_{0.565}]O_2$ with uniform particle size can be obtained by the synergistic dispersion of PVP and EG for the precursor formation.

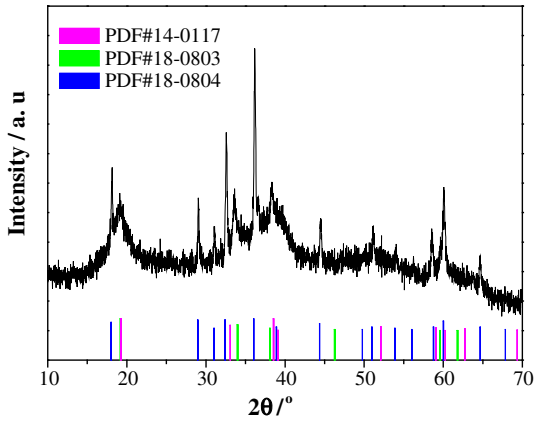

Fig. 2. XRD pattern of $Ni_{0.35}Mn_{0.65}(OH)_2$.

3.2. Electrochemical performance

Fig. 5 shows the charge/discharge curves of the cell $Li[Li_{0.131}Ni_{0.304}Mn_{0.565}]O_2$/Li between 3.0 V and 4.8 V at two temperatures under the same rate (0.1 C, where 1 C = 263 mAh g^{-1}). The charged $Li[Li_{0.131}Ni_{0.304}Mn_{0.565}]O_2$ can deliver a discharge capacity of 205 mAh g^{-1} with the charge–discharge efficiency of 74% at 25 °C. During the charging at the potential below 4.4 V, the capacity is contributed by the lithium de-intercalation from $Li[Li_{0.131}Ni_{0.304}Mn_{0.565}]O_2$, which is accompanied with the oxidation of Ni^{2+} for compensating charges [10]. When the charge potential is raised above 4.4 V, lithium ions can be further extracted from $Li[Li_{0.131}Ni_{0.304}Mn_{0.565}]O_2$ with simultaneous release of oxygen [14,23], which corresponds to the potential plateau around 4.5 V in Fig. 5. After the initial charging above 4.5 V, part of manganese ions are activated electrochemically due to the energetically favorable interstitial sites created by removal of lithium, so that the high-valence manganese could be reduced when the charged $Li[Li_{0.131}Ni_{0.304}Mn_{0.565}]O_2$ is discharged at the potential below 3.5 V [18]. From Fig. 5, it can be noted that the charged $Li[Li_{0.131}Ni_{0.304}Mn_{0.565}]O_2$ delivers a higher discharge capacity with a higher charge–discharge efficiency at 50 °C,

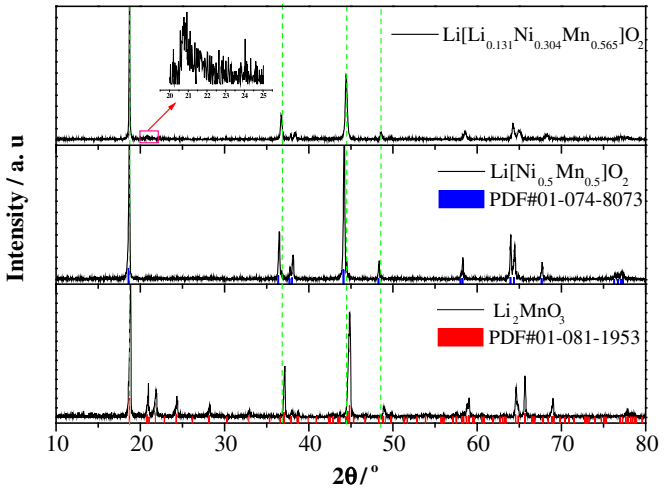

Fig. 3. XRD pattern of the prepared $Li[Li_{0.131}Ni_{0.304}Mn_{0.565}]O_2$, compared with $Li[Ni_{0.5}Mn_{0.5}]O_2$ and Li_2MnO_3.

Table 1
The peak positions of Li_2MnO_3, $Li[Li_{0.131}Ni_{0.304}Mn_{0.565}]O_2$ (Li-rich) and $Li[Ni_{0.5}Mn_{0.5}]O_2$.

Sample	2θ/°									
Li_2MnO_3	18.85	37.16	38.04	38.78	44.89	49.01	59.05	64.73	65.67	69.01
Li-rich	18.76	36.83	37.96	38.44	44.52	48.66	58.66	64.31	65.11	68.39
$Li[Ni_{0.5}Mn_{0.5}]O_2$	18.60	36.38	37.72	38.03	44.11	48.26	58.24	63.94	64.37	67.64

256 mAh g^{-1} with the efficiency of 79%. The increased capacity is mainly from the discharge below 3.5 V. This indicates that elevated temperature facilitates the extraction of lithium ions from $Li[Li_{0.131}Ni_{0.304}Mn_{0.565}]O_2$ and the stabilization of the lithium vacancies. At 50 °C, the discharge capacity of the prepared $Li[Li_{0.131}Ni_{0.304}Mn_{0.565}]O_2$ is also higher than that of the $Li[Li_{0.131}Ni_{0.304}Mn_{0.565}]O_2$ sample prepared by the co-precipitation method, in which not any dispersant was used and the particle size is non-uniform. For example, the sample prepared by co-precipitation of the hydrated metal nitrate salts with lithium hydroxide delivered a discharge capacity of 230 mAh g^{-1} in the region of 2.75–4.8 V [11]. This comparison suggests that the uniform particle size of $Li[Li_{0.131}Ni_{0.304}Mn_{0.565}]O_2$ favors the extraction of lithium ions from $Li[Li_{0.131}Ni_{0.304}Mn_{0.565}]O_2$, which is possibly associated with the homogeneous surface available on the size-uniform particles and thus less polarization.

The cyclic performance of $Li[Li_{0.131}Ni_{0.304}Mn_{0.565}]O_2$ was obtained through charge–discharge at 0.1 C between 3.0 V and 4.8 V, as shown in Fig. 6. It can be seen that the prepared $Li[Li_{0.131}Ni_{0.304}Mn_{0.565}]O_2$ retains a capacity of 178 mAh g^{-1} after 60 cycles, 87% of its initial discharge capacity. This performance is much better than those that have been reported in literature [31–33]. For example, the capacity retention of $Li[Li_{0.131}Ni_{0.304}Mn_{0.565}]O_2$ is 88% after 11 cycles [31], about 87% after 13 cycles [32] and about 85% after 25 cycles [33].

Although the prepared $Li[Li_{0.131}Ni_{0.304}Mn_{0.565}]O_2$ exhibits better elevated-temperature capacity and cyclic stability due to its uniform particle size, its capacity decay is still significant compared to the conventional cathode materials such as $LiCoO_2$ and $LiMn_2O_4$. The gradual capacity decay of lithium-rich oxide was attributed to the dissolution of transition metal ions induced through disproportionation reaction of Mn^{3+} to Mn^{4+} and Mn^{2+} [11]. To understand the mechanism on the capacity decay in more detail, the analyses on the variation of differential charge–discharge capacity (dQ/dV) with voltage were performed in this work.

Fig. 7 presents the charge–discharge curves of the cell $Li[Li_{0.131}Ni_{0.304}Mn_{0.565}]O_2$/Li at 0.05 C between 2.5 V and 4.8 V at

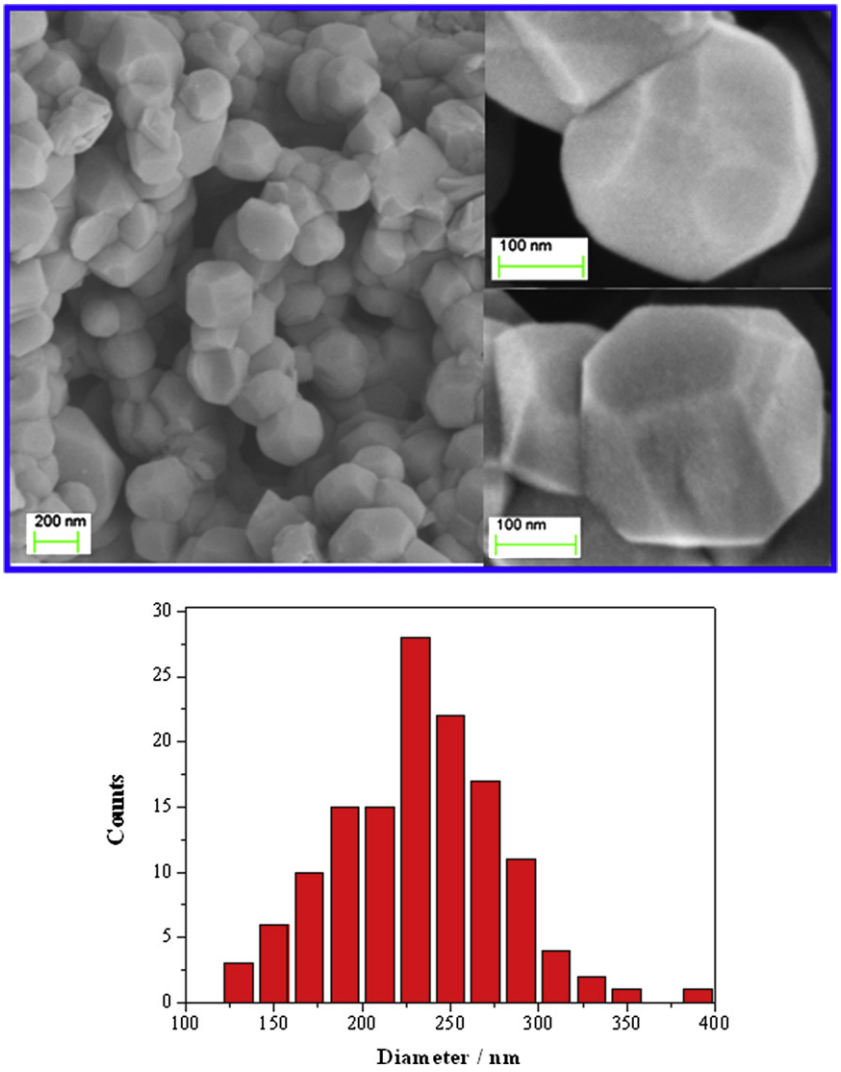

Fig. 4. SEM images and particle size distribution of the prepared $Li[Li_{0.131}Ni_{0.304}Mn_{0.565}]O_2$.

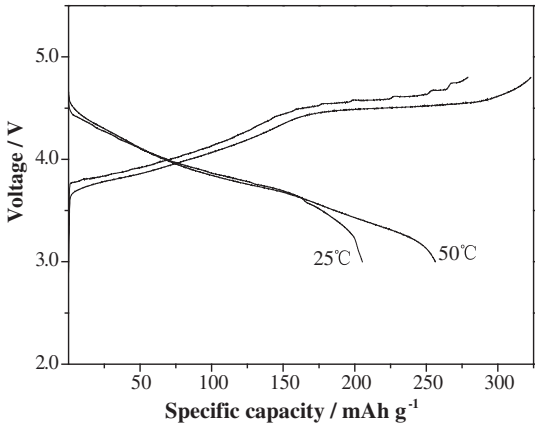

Fig. 5. Charge/discharge curves of the cell $Li[Li_{0.131}Ni_{0.304}Mn_{0.565}]O_2$/Li at 0.1 C.

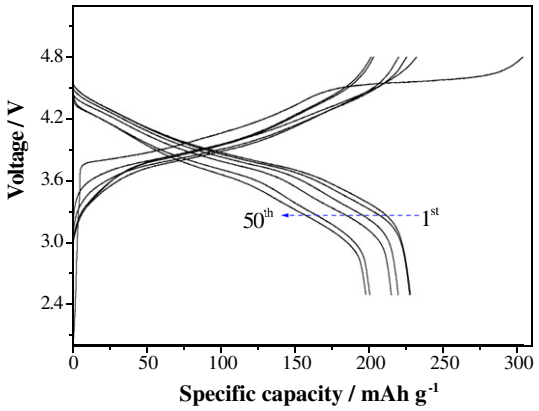

Fig. 7. Charge/discharge curves of the cell $Li[Li_{0.131}Ni_{0.304}Mn_{0.565}]O_2$/Li at 0.05 C between 2.5 V and 4.8 V.

25 °C for 1st, 2nd, 5th, 15th, 30th, and 50th cycles, and the corresponding d*Q*/d*V* curves are shown in Figs. 8 and 9. In 1st cycle (Fig. 8), the sharp oxidation peak at 4.56 V can be assigned to the irreversible oxidation of O^{2-} and the decomposition of electrolyte [34]. The weak reduction peak at 3.41 V is attributed to the reduction of manganese ions [31]. The oxidation peaks and reduction peaks between 3.5 V and 4.4 V can be attributed to the redox of Ni^{2+}/Ni^{4+} [31]. Why two oxidation peaks but three reduction peaks appear in 1st cycle for Ni^{2+}/Ni^{4+} couple can be explained by the structural rearrangement: two couple peaks around 3.8 V and 4.0 V are assigned to the redox of Ni^{2+}/Ni^{3+} and Ni^{3+}/Ni^{4+}, respectively, and can exist steadily in the charge–discharge region of 3.0 V and 4.4 V, which has been proved by Dahn [9]. However, as clearly seen from Fig. 9, the couple peaks around 4.0 V almost disappear after the charging above 4.5 V, and a couple peaks around 4.3 V appears subsequently, indicating that structural rearrangement induced by irreversible loss of oxygen has significant influence on the electronic environment of nickel ions with high valence.

After 1st cycle, the reduction peak current of manganese ions increases and its peak potential shifts negatively with cycling, and two oxidation peaks of manganese ion appear at 3.38 V and 3.06 V (Fig. 9). These phenomena are consistent with the observations from Ohzuku et al. [19]. However, no one has identified the reactions between 3.0 V and 3.5 V. Xu et al. [35] performed the EELS analysis of Mn-L edges of $Li[Li_{0.2}Ni_{0.2}Mn_{0.6}]O_2$ and showed that the oxidation states of manganese inside the cycled particles are almost identical with those of the pristine particles but the oxidation states of manganese on the surface of the cycled particles are lower. Boulineau et al. [29] and Xu et al. [35] have revealed a defect spinel-like phase at the edge of lithium-rich oxide particles after 1st charge to 4.8 V, based on the observation of STEM and EELS. With these results, we can infer that the reactions between 3.0 V and 3.5 V are related to the defect spinel-like phase and the changes of the peaks between 3.0 V and 3.5 V imply the local environment change of activated manganese ions during cycling.

Fig. 10 presents the variation of peak potentials of Ni^{2+}/Ni^{3+} and Ni^{3+}/Ni^{4+} with cycling. It can be seen that the peak potential difference of the two couples increases with cycling, 40 mV at 2nd cycle and 220 mV at 50th cycle for Ni^{2+}/Ni^{3+}, and 10 mV at 2nd cycle and 150 mV at 50th cycle for Ni^{3+}/Ni^{4+}. This indicates that insertion/extraction processes of lithium ions through Ni^{2+}/Ni^{4+} redox reactions become more irreversible with cycling. The equilibrium potentials of the two redox couples, which are related tightly with the structure of $Li[Li_{0.131}Ni_{0.304}Mn_{0.565}]O_2$, can be estimated by the average value of oxidation peak potentials and reduction peak potentials. As shown in Fig. 10, the equilibrium potentials of Ni^{2+}/Ni^{3+} and Ni^{3+}/Ni^{4+} change with cycling, suggesting that the structural rearrangement proceeds into the bulk of $Li[Li_{0.131}Ni_{0.304}Mn_{0.565}]O_2$. The rearrangement can be understood as the result of the Li/Ni exchange in metal layers and lithium layers. Ni ions occupied in lithium layers block the pathway of Li^+ diffusion, and thus increase the energy barrier of Li^+ insertion/desertion. Consequently, the polarization of Li^+ insertion/desertion in Li

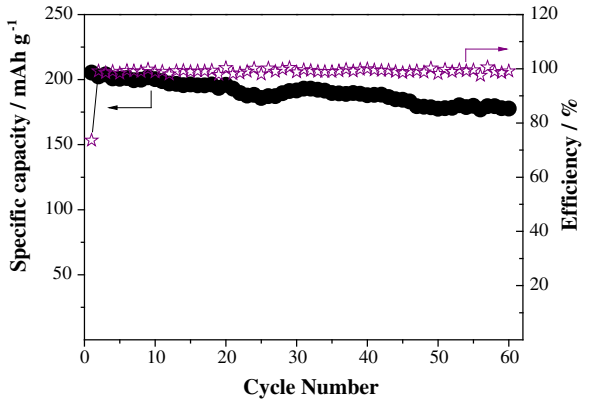

Fig. 6. Cyclic performance of the cell $Li[Li_{0.131}Ni_{0.304}Mn_{0.565}]O_2$/Li at 0.1 C between 3.0 V and 4.8 V at 25 °C.

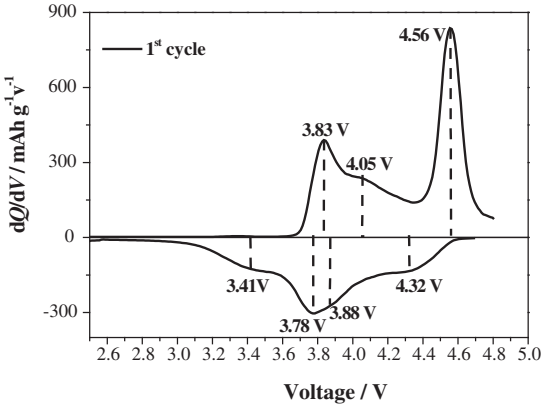

Fig. 8. d*Q*/d*V* (*vs.* voltage) curves of $Li[Li_{0.131}Ni_{0.304}Mn_{0.565}]O_2$ at 1st cycle, calculated from the data of Fig. 7.

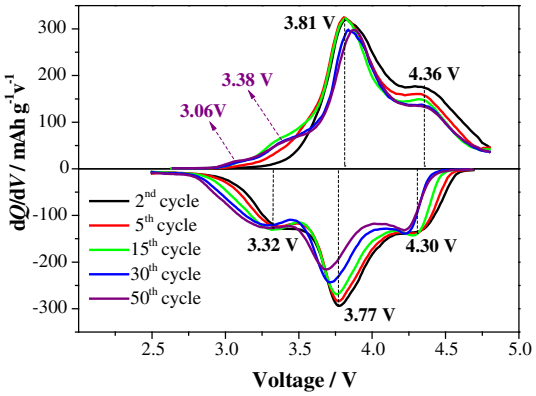

Fig. 9. dQ/dV (*vs.* voltage) curves of $Li[Li_{0.131}Ni_{0.304}Mn_{0.565}]O_2$ at 2nd, 5th, 15th, 30th, and 50th cycle, calculated from the data of Fig. 7.

$[Li_{0.131}Ni_{0.304}Mn_{0.565}]O_2$ increases, leading to the capacity decay of $Li[Li_{0.131}Ni_{0.304}Mn_{0.565}]O_2$.

Therefore, the capacity decay of $Li[Li_{0.131}Ni_{0.304}Mn_{0.565}]O_2$ results from, not only the loss of active material caused by the solubility of transition metal ions, but also the polarization of Li^+ insertion/desertion induced by structural rearrangement.

Fig. 11 presents the rate capability of the prepared Li $[Li_{0.131}Ni_{0.304}Mn_{0.565}]O_2$. The sample delivers 170 mAh g^{-1} at 0.2 C, 145 mAh g^{-1} at 0.5 C, 130 mAh g^{-1} at 1 C, and 22 mAh g^{-1} at 5 C. Compared with the other $Li[Li_{0.131}Ni_{0.304}Mn_{0.565}]O_2$ samples prepared by co-precipitation without any dispersant [36], our sample exhibits better rate performance. However, the rate capacity is still poor compared with conventional cathode materials of lithium ion battery, such as $LiCoO_2$ and $LiMn_2O_4$. The poor rate capacity of Li

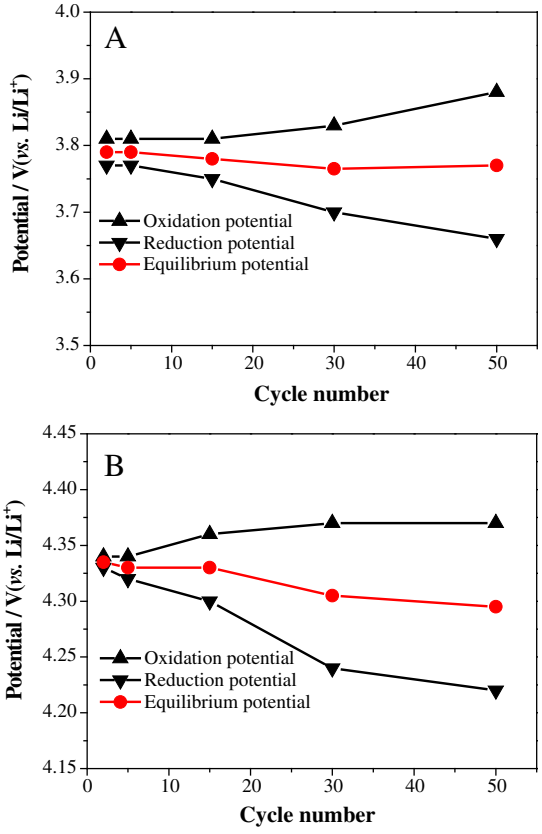

Fig. 10. Variation of peak potentials of Ni^{2+}/Ni^{3+} (A) and Ni^{3+}/Ni^{4+} (B) with cycling.

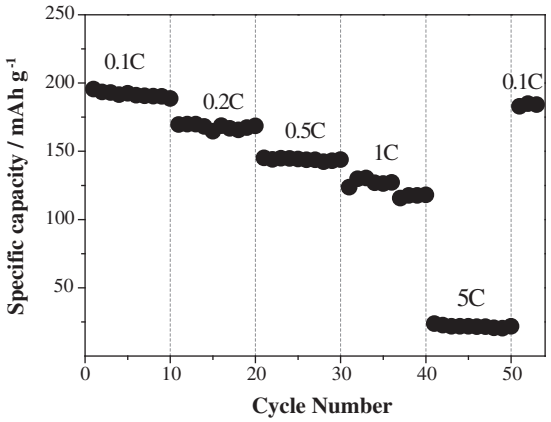

Fig. 11. Cyclic performance of the cell $Li[Li_{0.131}Ni_{0.304}Mn_{0.565}]O_2$/Li at different charge/discharge rates between 3.0 V and 4.8 V.

$[Li_{0.131}Ni_{0.304}Mn_{0.565}]O_2$ is related to the low electronic conductivity associated with the Mn^{4+} ions and the thick SEI layer formed by a reaction of the cathode with the electrolyte [34]. Fortunately, it has been known that the poor rate capacity of $Li[Li_{0.131}Ni_{0.304}Mn_{0.565}]O_2$ can be improved by coating such as carbon and Al_2O_3 [37–39].

4. Conclusions

In this paper, we report a new method to prepare Li $[Li_{0.131}Ni_{0.304}Mn_{0.565}]O_2$, in which polyvinylpyrrolidone (PVP) and ethylene glycol (EG) are used as dispersants. With the synergistic dispersion of PVP and EG, size-uniform $Li[Li_{0.131}Ni_{0.304}Mn_{0.565}]O_2$ particle can be obtained. The obtained $Li[Li_{0.131}Ni_{0.304}Mn_{0.565}]O_2$ delivers a high discharge capacity, and exhibits good cyclic stability and rate performance. The capacity decay mechanism of lithium-rich layered oxide was also electrochemically understood in more detail. The results imply that the capacity decay of Li $[Li_{0.131}Ni_{0.304}Mn_{0.565}]O_2$ results from not only the loss of active material caused by the solubility of transition metal ions, but also the polarization of Li^+ insertion/desertion induced by structural rearrangement.

Acknowledgment

The authors are highly grateful for the financial support from by the joint project of National Natural Science Foundation of China and Natural Science Foundation of Guangdong Province (Grant No. U1134002), the National Natural Science Foundation (Grant No. 21273084), the Natural Science Fund of Guangdong Province (Grant No. 10351063101000001), and the key project of Science and Technology in Guangdong Province (Grant No. 2012A010702003).

References

[1] F.Y. Cheng, J. Liang, Z.L. Tao, J. Chen, Adv. Mater. 23 (2011) 1695–1715.
[2] O.K. Park, Y. Cho, S. Lee, H.-C. Yoo, H.-K. Song, J. Cho, Energy Environ. Sci. 4 (2011) 1621–1633.
[3] P. He, H. Wang, L. Qi, T. Osaka, J. Power Sources 158 (2006) 529–534.
[4] J.-Y. Luo, H.-M. Xiong, Y.-Y. Xia, J. Phys. Chem. C 112 (2008) 12051–12057.
[5] K. Katakura, K. Wada, Y. Kajiki, A. Yamamoto, Z. Ogumi, J. Power Sources 189 (2009) 240–247.
[6] S. Beninati, L. Damen, M. Mastragostino, J. Power Sources 194 (2009) 1094–1098.
[7] M.-H. Lee, Y.-J. Kang, S.-T. Myung, Y.-K. Sun, Electrochim. Acta 50 (2004) 939–948.
[8] Z.H. Lu, D.D. MacNeil, J.R. Dahn, Electrochem. Solid-State Lett. 4 (2001) A191–A194.
[9] Z.H. Lu, L.Y. Beaulieu, R.A. Donaberger, C.L. Thomas, J.R. Dahn, J. Electrochem. Soc. 149 (2002) A778–A791.

[10] M.M. Thackeray, S.-H. Kang, C.S. Johnson, J.T. Vaughey, R. Benedek, S.A. Hackney, J. Mater. Chem. 17 (2007) 3112–3125.
[11] C.S. Johnson, N. Li, C. Lefief, M.M. Thackeray, Electrochem. Commun. 9 (2007) 787–795.
[12] K.A. Jarvis, Z.Q. Deng, L.F. Allard, A. Manthiram, P.J. Ferreira, Chem. Mater. 23 (2011) 3614–3621.
[13] J.-L. Liu, J. Wang, Y.-Y. Xia, Electrochim. Acta 56 (2011) 7392–7396.
[14] A.R. Armstrong, M. Holzapfel, P. Novák, C.S. Johnson, S.-H. Kang, M.M. Thackeray, P.G. Bruce, J. Am. Chem. Soc. 128 (2006) 8694–8698.
[15] S.-H. Kang, Y.K. Sun, K. Amine, Electrochem. Solid-State Lett. 6 (2003) A183–A186.
[16] M. Jiang, B. Key, Y.S. Meng, C.P. Grey, Chem. Mater. 21 (2009) 2733–2745.
[17] J. Jiang, J.R. Dahn, Electrochim. Acta 50 (2005) 4778–4783.
[18] Y.J. Hong, J.H. Kim, M.H. Kim, Y.C. Kang, Mater. Res. Bull. 47 (2012) 2022–2026.
[19] T. Ohzuku, M. Nagayama, K. Tsuji, K. Ariyoshi, J. Mater. Chem. 21 (2011) 10179–10188.
[20] Z.Q. Deng, A. Manthiram, J. Phys. Chem. C 115 (2011) 7097–7103.
[21] Y. Wu, A. Manthiram, Electrochem. Solid-State Lett. 10 (2007) A151–A154.
[22] J. Bareño, C.H. Lei, J.G. Wen, S.-H. Kang, I. Petrov, D.P. Abraham, Adv. Mater. 22 (2010) 1122–1127.
[23] Z.H. Lu, J.R. Dahn, J. Electrochem. Soc. 149 (2002) A815–A822.
[24] J. Bréger, M. Jiang, N. Dupre, Y.S. Meng, S.-H. Yang, G. Ceder, C.P. Grey, J. Solid State Chem. 178 (2005) 2575–2585.
[25] G.Z. Wei, X. Lu, F.-S. Ke, L. Huang, J.-T. Li, Z.-X. Wang, Z.-Y. Zhou, S.-G. Sun, Adv. Mater. 22 (2010) 4364–4367.
[26] J. Wang, X.Y. Yao, X.F. Zhou, Z.P. Liu, J. Mater. Chem. 21 (2011) 2544–2549.
[27] D.A.R. Barkhouse, J.R. Dahn, J. Electrochem. Soc. 152 (2005) A746–A751.
[28] C.H. Lei, J. Bareño, J.G. Wen, I. Petrov, S.-H. Kang, D.P. Abraham, J. Power Sources 178 (2008) 422–433.
[29] A. Boulineau, L. Simonin, J.-F. Colin, E. Canévet, L. Daniel, S. Patoux, Chem. Mater. 24 (2012) 3558–3566.
[30] F. Amalraj, D. Kovacheva, M. Talianker, L. Zeiri, J. Grinblat, N. Leifer, G. Goobes, B. Markovsky, D. Aurbach, J. Electrochem. Soc. 157 (2010) A1121–A1130.
[31] C.S. Johnson, J.-S. Kim, C. Lefief, N. Li, J.T. Vaughey, M.M. Thackeray, Electrochem. Commun. 6 (2004) 1085–1091.
[32] D. Li, F. Lian, W.H. Qiu, F.S. Li, K.-C. Chou, Adv. Mater. Res. 347–353 (2012) 3518–3521.
[33] J.-S. Kim, C.S. Johnson, J.T. Vaughey, M.M. Thackeray, J. Power Sources 153 (2006) 258–264.
[34] A. Manthiram, J. Phys. Chem. Lett. 2 (2011) 176–184.
[35] B. Xu, C.R. Fell, M.F. Chi, Y.S. Meng, Energy Environ. Sci. 4 (2011) 2223–2233.
[36] C.R. Fell, K.J. Carroll, M.F. Chi, Y.S. Meng, J. Electrochem. Soc. 157 (2010) A1202–A1211.
[37] J. Liu, Q.Y. Wang, B. Reeja-Jayan, A. Manthiram, Electrochem. Commun. 12 (2010) 750–753.
[38] W.C. West, J. Soler, M.C. Smart, B.V. Ratnakumar, S. Firdosy, V. Ravi, M.S. Anderson, J. Hrbacek, E.S. Lee, A. Manthiram, J. Electrochem. Soc. 158 (2011) A883–A889.
[39] Y. Wu, A. Manthiram, Electrochem. Solid-State Lett. 9 (2006) A221–A224.